



A PAndAS view of the resolved stellar populations in M31 dwarf elliptical satellites

D. Crnojević¹ and The PAndAS collaboration

¹ Institute for Astronomy, University of Edinburgh, Royal Observatory, Blackford Hill, EH9 3HJ Edinburgh, UK, e-mail: dc@roe.ac.uk

Abstract. We present the first truly global view of the closest elliptical galaxies, the dwarf elliptical (dE) companions of M31 NGC147 and NGC185. We exploit the deep PAndAS photometric dataset in order to investigate the resolved stellar content and structure of these dEs out to larger distances than ever previously probed. From the analysis of their old red giant branch stars, we derive density maps, full surface brightness profiles and metallicity distribution functions. We find that NGC147 shows pronounced tidal tails likely due to its interaction with M31, while NGC185 retains a regular elliptical shape over its entire extent. The two dEs follow a Sersic profile out to ~ 5 kpc, and the effective radii derived in this study are a factor of two larger than previous literature values. While NGC185 shows a significant gradient in metallicity (~ -0.05 dex/kpc), this is almost absent in NGC147. The detailed understanding of nearby dEs is crucial for the studies of more distant objects, and we discuss how internal and environmental processes could have influenced the evolution of NGC147 and NGC185 in light of our results.

Key words. Galaxies: dwarf – Galaxies: stellar content – Galaxies: photometry – Galaxies: Local Group – Galaxies: individual: NGC185, NGC147

1. Introduction

Dwarf galaxies, despite their modest size, have surprisingly turned out to be critical objects for our understanding of the Λ CDM cosmology on small scales, and for investigating the relative role played by internal and external processes in galaxy evolution. In particular, the formation and evolution of dwarf elliptical (dE) galaxies remains an intriguing open question. The only examples of this class of dwarfs in the Local Group are the dE satellites of M31. NGC147 and NGC185 have similar luminosities and metallicity content but present otherwise stunning differences in their recent evolutionary history (NGC185 contains gas,

dust and young stars as opposed to NGC147; e.g., Geha et al. 2010, and references therein). They are thus particularly interesting targets to test the predictions of cosmological models on galaxy evolution, but so far limited field-of-view studies have precluded a *global* understanding of their properties. In this contribution, we present the first deep, homogeneous wide-field view of the resolved stellar populations in these dEs.

2. Data and colour-magnitude diagrams

We use data from the Pan-Andromeda Archeological Survey (PAndAS,

McConnachie et al. 2009), a wide-field survey covering an area of ~ 150 kpc around M31, thus comprising the vast majority of its known satellites. The observations are taken with MegaCam on the CFHT in the g and i filters, and the data are processed as detailed in McConnachie et al. (2009); Richardson et al. (2011). PSF photometry has been performed on the images and resolves the uppermost ~ 3 mag of the red giant branch (RGB) for the target galaxies, with a signal-to-noise ratio of 5 at $g \sim 24$ and $i \sim 25$. We adopt the distances of the dEs as derived by Conn et al. (2012), and we recompute position angle and ellipticity from our data.

We consider a region of $\sim 1 \times 1$ deg² around each of NGC147 and NGC185 for our subsequent analysis. The colour-magnitude diagrams (CMDs) of the target dEs are presented in Fig. 1, after having been dereddened on a star-by-star basis adopting the Schlegel reddening maps (Schlegel et al. 1998). The CMDs show a prominent, old RGB as the dominant feature, at colours $(g-i)_0 \sim 1$. At magnitudes brighter than the tip of the RGB (TRGB), two diagonal sequences comprise mainly foreground M- and K-dwarfs belonging to the disk and the halo of our Galaxy. Luminous asymptotic giant branch (AGB) stars also lie in this region of the CMD, but in optical bands the contamination from foreground stars is too strong to study these intermediate-age ($\sim 0.5 - 8$ Gyr) populations. Near-infrared filters can be employed in order to more easily separate genuine AGB stars from Galactic stars (Rejkuba et al. 2006; Crnojević et al. 2011), and will be the subject of a forthcoming paper (Crnojević et al., in prep.).

3. Spatial analysis

We select RGB stars with magnitudes fainter than the TRGB and brighter than $i_0 = 23.5$ (this limit has been chosen in order to avoid decreasing completeness and increasing contamination from unresolved background galaxies), and derive density maps. Fig. 2 shows the first, striking difference between the two target dEs. While NGC185 retains a regular, elliptical shape out to the furthest radii considered,

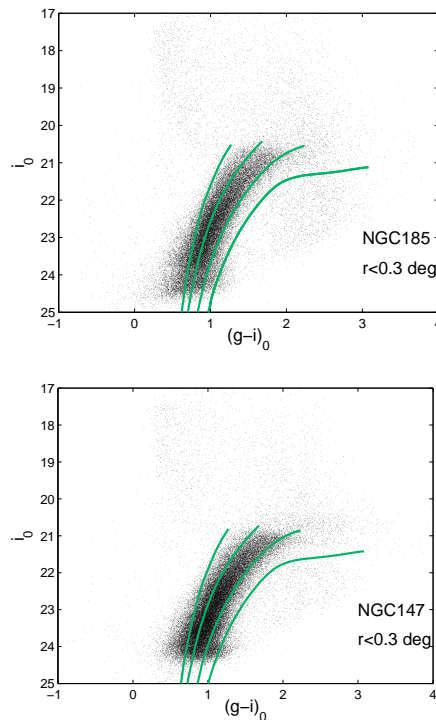


Fig. 1. Dereddened CMDs of NGC185 and NGC147 (for all stars with an elliptical radius smaller than 0.3 deg). We overplot Dartmouth isochrones with a fixed age of 12 Gyr and varying metallicity ($[\text{Fe}/\text{H}] = -1.5, -1.3, -0.7$ and -0.3 , from left to right) to underline the position of the RGB. The two bright, diagonal sequences above the RGB consist of Galactic foreground stars.

NGC147's isophotes are clearly twisting in the NW-SE direction. This dE has been recently shown to have extended tidal tails which possibly result from a tidal interaction with M31 (Irwin et al., in prep.).

We further derive surface brightness profiles in the following way. For the central regions ($r \lesssim 0.15$ deg), where stellar crowding is high and the completeness of the resolved stellar photometry low, we employ diffuse light in order to trace the surface brightness. On the other hand, with increasing galactocentric radius the surface brightness becomes progressively lower, and individual RGB star counts are more powerful to measure the dEs' profiles.

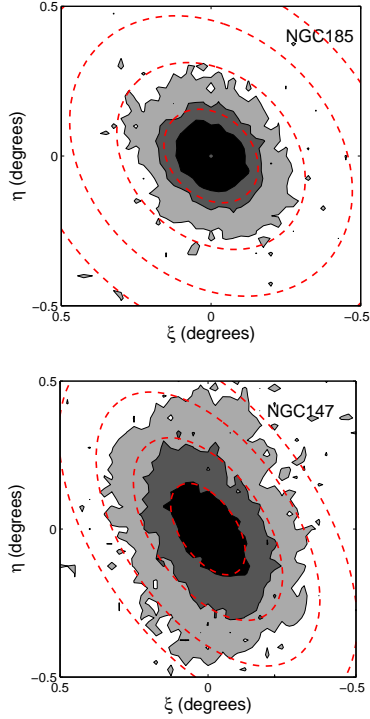


Fig. 2. RGB density maps, with logarithmically spaced isodensity contours (at 4, 16 and 64 stars per arcmin²). Equally spaced ellipses with the average position angle and ellipticity of each galaxy are drawn as a reference (at radii of 0.175, 0.35, 0.525 and 0.7 deg).

We then combine the two methods by scaling the resolved RGB number density profiles to the surface brightness profiles in the radial range where they overlap. For the first time, we obtain a full radial profile for the target dEs that extends all the way out to 0.7 deg, reaching magnitudes as faint as $\mu_g \sim 32$ mag/arcsec².

Note that the contamination in the observed CMDs comprises unresolved background galaxies, M31 halo stars and foreground Galactic stars, the latter being the most numerous. In order to carefully take this into account, we estimate the number density of contaminants that fall within our RGB selection box from two large (~ 3.8 deg²) field regions separated from the dEs by ~ 1 deg. We then subtract the field number counts from the

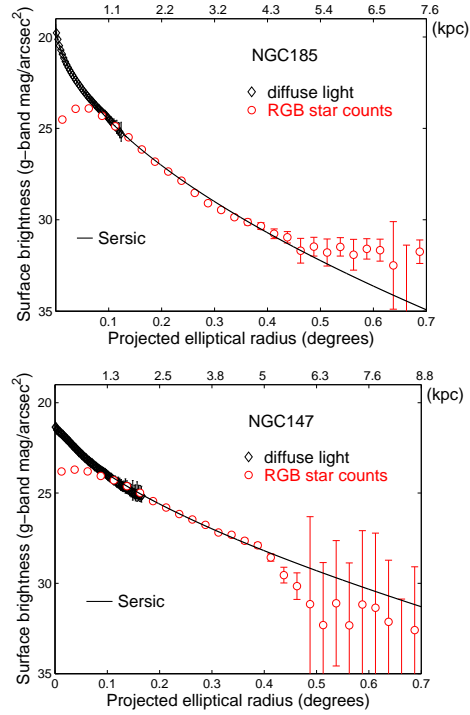


Fig. 3. Combined surface brightness profiles as a function of projected elliptical radius, derived from diffuse light in the innermost regions (black diamonds) and from RGB resolved star counts in the outer regions (red circles). The profiles have been subtracted for background/foreground contamination. For NGC147, we show the profile along the major axis, i.e. the direction free from tidal tails. The upper axes indicate distances in kpc units. The solid lines are the best-fit Sersic profiles to the data.

resolved RGB number density profiles, before combining them to the central diffuse light profiles. Finally, for NGC147 we only take into account the profile along the major axis, i.e. in the direction free from tidal tails. In Fig. 3 we show the resulting surface brightness profiles, and fit them with a Sersic profile (Sersic 1968) (the best-fit values are reported in Tab. 1). NGC185 is brighter in the central regions, and overall shows a steeper profile than NGC147. The profiles for both galaxies closely follow a Sersic profile out to a radius of ~ 5 kpc. While the surface brightness of NGC147 drops at larger

Table 1. Best-fit Sersic parameters to the derived surface brightness profiles.

	NGC147	NGC185
n	1.57 ± 0.03	1.78 ± 0.02
$r_{\text{eff}} (')$	6.18 ± 0.07	2.94 ± 0.04
$r_{\text{eff}} (\text{kpc})$	1.30 ± 0.02	0.53 ± 0.01

galactocentric distances (in the tidal tail-free direction), NGC185 shows an excess of RGB counts beyond this radius, however this is still within 2σ of the field contamination level. We underline that the derived effective radii (Tab. 1) are larger by a factor of ~ 2 with respect to any previous study of these dEs (e.g., Battinelli & Demers 2004b,a; Geha et al. 2010, and references therein).

4. Metallicity distribution functions

By assuming that the old RGB stars are coeval, it is possible to compute photometric metallicity distribution functions (MDFs) via isochrone interpolation (Harris et al. 1999; Crnojević et al. 2010). We adopt Dartmouth solar-scaled isochrones (Dotter et al. 2008) with a fixed age of 12 Gyr and varying metallicity ($[\text{Fe}/\text{H}] = -2.5$ to -0.3 , see also Fig. 1) and derive a metallicity value for each individual RGB star. We adopt the same procedure for the contaminant sources in our field regions that fall within the RGB box, even though these are not strictly speaking real MDFs. We then subtract the contaminants distribution functions to the dEs' MDFs. The average metallicities of the two target galaxies are $\langle[\text{Fe}/\text{H}]\rangle = -1.08 \pm 0.39$ for NGC185 and $\langle[\text{Fe}/\text{H}]\rangle = -0.96 \pm 0.30$ for NGC147 (mean value and internal dispersion are derived via Gaussian fitting). These values are consistent with previous spectroscopic measurements of these dwarfs (e.g. Geha et al. 2010).

The resulting MDFs are displayed in Fig. 4, where we divide each dE in three equally spaced radial steps. Note that we are excluding the innermost 0.175 deg from our analysis because of incompleteness in the stellar photometry. The radial MDFs for

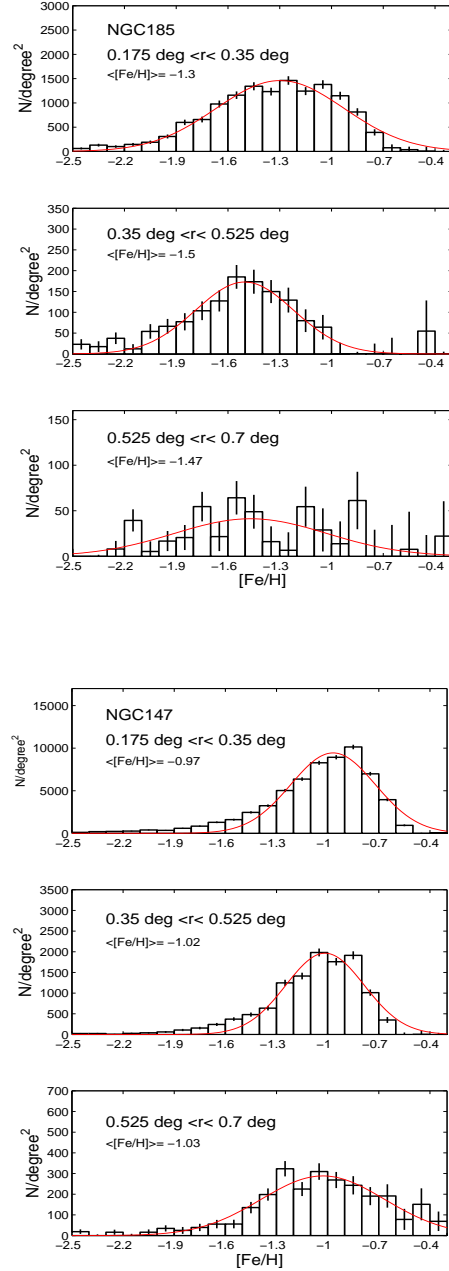


Fig. 4. Photometric MDFs (per unit area) in different radial bins for the target dEs. We derive MDFs for RGB stars via isochrone interpolation (see text for details), and subsequently subtract the background/foreground contamination. Gaussians are fitted to derive mean metallicities, which are reported in each subpanel.

NGC185 show a steep gradient in the first two bins (~ -0.05 dex/kpc), while the last one is dominated by noise. On the contrary, NGC147's average metallicity does not significantly change within the considered radial range (~ -0.008 dex/kpc).

5. Discussion and conclusions

We have exploited the PAndAS photometric dataset in order to obtain the first deep, wide-field view of the closest elliptical galaxies, NGC185 and NGC147. We obtain resolved stellar photometry out to radii significantly larger than ever previously probed for these galaxies (Battinelli & Demers 2004b,a; Geha et al. 2010). The CMDs of the target dwarfs show the uppermost ~ 3 mag of the RGB, and we use these old stars to trace the *global* spatial structure and metallicity content of the dEs.

RGB density maps disclose the disrupting nature of NGC147, in stark contrast with the regular elliptical shape of NGC185 out to the outermost radii considered. For the first time, we derive full surface brightness profiles by combining diffuse light in the central parts and RGB stellar counts in the outer galaxy regions, reaching magnitudes as faint as $\mu_g \sim 32$ mag/arcsec². Our targets' profiles follow a Sersic law out to ~ 5 kpc. We furthermore derive effective radius values that turn out to be twice as large as any previous literature results.

The clearly different interaction history that the two dwarfs experienced can be linked to their metallicity content. We derive photometric MDFs for RGB stars, and look for trends in their radial properties. Strikingly enough, NGC185 shows a steep gradient while the average metallicity remains almost constant throughout the whole body of NGC147. These dEs have also been recently shown to

have a similar degree of rotation (Geha et al. 2010). In light of this, we deem it likely that the difference in the radial metallicity gradient between the two dEs, together with the different slopes of their surface brightness profiles, derive from their past interaction history rather than from internal effects (e.g. rotation). The results presented in this contribution are fully described in Crnojević et al., MNRAS, submitted.

Acknowledgements. I wish to thank the organizers for such a stimulating and enjoyable Symposium. DC is supported by an STFC Rolling Grant.

References

- Battinelli, P. & Demers, S. 2004a, A&A, 418, 33
- Battinelli, P. & Demers, S. 2004b, A&A, 417, 479
- Conn, A. R., Ibata, R. A., Lewis, G. F., et al. 2012, ApJ, 758, 11
- Crnojević, D., Grebel, E. K., & Koch, A. 2010, A&A, 516, A85
- Crnojević, D., et al. 2011, A&A, 530, A58
- Dotter, A., Chaboyer, B., Jevremović, D., et al. 2008, ApJS, 178, 89
- Geha, M., van der Marel, R. P., Guhathakurta, P., et al. 2010, ApJ, 711, 361
- Harris, G. L. H., Harris, W. E., & Poole, G. B. 1999, AJ, 117, 855
- McConnachie, A. W., Irwin, M. J., Ibata, R. A., et al. 2009, Nature, 461, 66
- Rejkuba, M., et al. 2006, A&A, 448, 983
- Richardson, J. C., Irwin, M. J., McConnachie, A. W., et al. 2011, ApJ, 732, 76
- Schlegel, D. J., Finkbeiner, D. P., & Davis, M. 1998, ApJ, 500, 525
- Sersic, J. L. 1968, Atlas de galaxias australes, (Observatorio Astronomico, Cordoba, Argentina)